AMERICAN METEOROLOGICAL SOCIETY
AMS Journals Online

AMS Home   Journals Home   Journal Archive   Subscribe   For Authors   Help   Advanced Search   [Search] Go

Full Text View

Numerical Experiments on the Breaking of Solitary Internal Wavesover a Slope–Shelf Topography

Vasiliy Vlasenko and Kolumban Hutter

Institut für Mechanik, Technische Universität Darmstadt, Darmstadt, Germany

ABSTRACT

A theoretical study of the transformation of large amplitude internal solitary waves (ISW) of permanent form over a slope–shelf topography is considered using as basis the Reynolds equations. The vertical fluid stratification, amplitudes of the propagating ISWs, and the bottom parameters were taken close to those observed in the Andaman and Sulu Seas. The problem was solved numerically.

It was found that, when an intense ISW of depression propagates from a deep part of a basin onto the shelf with water depth H_s, a breaking event will arise whenever the wave amplitude a_m is larger than $0.4(H_s - H_m)$, where H_m is the undisturbed depth of the isopycnal of maximum depression. The cumulative effect of nonlinearity in a propagating ISW leads to a steepening and overturning of a rear wave face over the inclined bottom. Immediately before breaking the horizontal orbital velocity at the site of instability exceeds the phase speed of the ISW. So, the strong breaking is caused by a kinematic instability of the propagating wave. At the latest stages of the evolution the overturned hydraulic jump transforms into a horizontal density intrusion (turbulent pulsating wall jet) propagating onto the shelf.

The breaking criterion of the ISW over the slope was found. Over the range of examined parameters ($0.52° < \gamma < 21.8°$, where γ is the slope angle) the breaking event arises at the position with depth H_b, when the nondimensional wave amplitude $\bar{a} = a_m/(H_b - H_m)$ satisfies the condition $\bar{a} \cong 0.8°/\gamma + 0.4$. If the water depth H_s on a shelf is less than H_b, a solitary wave breaks down before it penetrates into a shallow water zone; otherwise (at $H_s > H_b$) it passes as a dispersive wave tail onto the shelf without breaking.

Options:
- Create Reference
- Email this Article
- Add to MyArchive
- Search AMS Glossary

Search CrossRef for:
- Articles Citing This Article

Search Google Scholar for:
- Vasiliy Vlasenko
- Kolumban Hutter

1. Introduction

Numerous in situ and remote-sensing observations demonstrate the evidence of internal solitary waves (ISW) and wave trains in marginal seas, straits, and coastal waters (for a detailed review see, for instance, Ostrovsky and Stepanynts 1989;

Apel et al. 1995). It is generally accepted that one of the main causes of internal waves is due to a barotropic tide interacting with the submarine topography. This generation mechanism is basically recognized (Lee and Beardsley 1974; Maxworthy 1979; Vlasenko 1992; Lamb 1994; Gerkema and Zimmerman 1995), but the structure of highly nonlinear internal waves and their ultimate fate remain comparatively poorly understood when they propagate as solitary waves toward shore into shoaling regions. At the same time observations of internal waves in the Andaman (Osborne and Burch 1980) and Sulu Sea (Apel et al. 1985), in the Massachusetts Bay (Halpern 1971), and on the Australian North West Shelf (Holloway et al. 1997) have shown that shoaling effects and local change of the bottom topography may essentially influence the evolution and the dynamics of ISWs.

The most popular interpretation of the behavior of intense internal waves is based on the weakly nonlinear theories developed for deep (Benjamin 1967; Ono 1975), finite (Joseph 1977; Kubota et al. 1978), or shallow water basins (Benjamin 1966; Benny 1966). When applied to the evolution over variable bottom topography (Holloway et al. 1997; Liu 1988; Liu et al. 1998) the weakly nonlinear theories of internal waves are not sufficiently advanced to answer a variety of important questions relevant to the strong overturning and breaking of intense internal waves. The main problem with such an approach is that the nonlinear advection and dispersion coefficients estimated from observational data, assumed small, are often not really small, and theories fail to describe the large amplitude ISW (with amplitudes up to 100 m and more) observed, for instance in the Andaman Sea (Perry and Schimke 1965; Osborne and Burch 1980), in the Sulu Sea (Apel et al. 1985; Liu et al. 1985), at the Mascarene Ridge (Sabinin 1992; Konyaev et al. 1995), near the Strait of Gibraltar (Bockel 1962; Bryden et al. 1994), and in the central Bay of Biscay (New and Pingree 1990). Probably for this reason, there is still no satisfactory theoretical description of the experimental data obtained in the Sulu Sea (Chapman et al. 1991) and the Pechora Sea (Serebryany and Shapiro 2000) on the breaking of oceanic internal solitary waves. The strong nonlinearity demands an appropriate theoretical description either on the basis of revised weakly nonlinear theories, which include higher-order nonlinearities (see, e.g., Grimshaw et al. 1999; Holloway et al. 1999; Stanton and Ostrovsky 1998), or a complete system of equations that takes into account the full nonlinearities of the wave motion.

Several laboratory studies have been performed on the overturning and breaking of internal waves over bottom topography. It was found by Cacchione and Wunsch (1974) and Ivey and Nokes (1989) that horizontally propagating periodic waves produce an instability and mixing in the bottom boundary layer above the slope. Mixing is most intense when the slope is at the critical angle. Recently, Thorpe (1999) predicted theoretically the excitation of alongshore residual currents of several centimeters per second that are produced by the interaction of incident and reflected waves. In laboratory works of Wallace and Wilkinson (1988) and De Silva et al. (1997) on the breaking of periodic internal waves over a sloping bottom the formation of turbulent intrusions of dense water was observed that propagated up the slope until it was eventually dissipated by friction.

Weak shearing and strong breaking (overturning) instabilities depending on the incident wave amplitude and on stratification were observed in experiments of Helfrich et al. (1984) and Helfrich and Melville (1986), who considered the scattering and breaking of solitary waves over a gradually varying change in water depth. They supposed that the strong breaking mechanism is a kinematic instability rather than a shear instability, as was also concluded by Kao et al. (1985). This result was further confirmed in experimental work by Grue et al. (2000). In some cases the instability of the internal wave leads to the generation of high baroclinic modes. It was found first by Helfrich (1992) and recently by Michallet and Ivey (1999) that shoaling of a solitary internal wave results in wave breaking and production of multiple soliton-like waves of elevation (turbulent surges or boluses) that propagate up the slope.

Laboratory experiments on the interaction of solitary internal waves with a sill were also performed to study the energy loss caused by the interaction (Diebels et al. 1994; Maurer et al. 1996; Wessels and Hutter 1996). It was found that the ratio of the sill height to the thickness of the lower layer was the decisive parameter controlling the amount of transmitted and reflected energy. At certain critical conditions the solitary wave breaks apart and produces a horizontal turbulent density intrusion (Wessels and Hutter 1996).

Nevertheless, one should note that the laboratory results obtained on the dynamics of internal waves over bottom topography cannot directly be applied to oceanic conditions because of the essentially different spatial and temporal scales of the phenomenon in the laboratory and in the ocean. So, the present paper was motivated by the fact that so far there is not sufficient clarity in the understanding of the breaking mechanism of large-amplitude oceanic ISWs propagating from the deep part of the ocean onto a shelf. Existing numerical nonhydrostatic models (Saffarinia and Kao 1996; Terez and Knio 1998), developed in the frame of the Navier-Stokes equations to study strong solitary internal waves, were applied to laboratory conditions. The mechanism and the criterion of internal wave breaking over the inclined bottom was not obtained and not discussed in those papers. In the present paper a numerical model of internal wave transformation over the inclined bottom based on the full system of Reynolds equations is developed and applied for the conditions of the Andaman and Sulu Seas.

The paper is organized as follows: The mathematical model is presented in section 2. The initialization of the model and relevant parameters are discussed in section 3. Section 4 is devoted to the description of numerical results. Here the mechanism of breaking and the breaking criterion are discussed in detail. A summary and conclusions are given in section 5.

2. Numerical model

A nonlinear numerical model with continuous vertical stratification and turbulent exchange has been developed to describe the interaction of internal waves with a variable bottom topography. The model assumes a plane solitary wave of depression with amplitude a_m, whose vertical structure is defined by buoyancy frequency profiles, for example, as depicted in Fig. 1b

○; such a wave propagates normally from the deep part I with depth H_1 (Fig. 1a ○) to the linear continental slope II and farther to the shelf III. The objective of our modeling efforts was to investigate the process of evolution of a solitary internal wave in regions II and III during its strong overturning and breaking.

A two-dimensional Cartesian x–z coordinate system is used in which the x axis lies at the undisturbed free surface and the z axis is vertical opposite to the direction of gravity. In this frame, the system of Reynolds equations, written for the streamfunction $\psi(x, z, t)$ ($u = \psi_z$, $w = -\psi_x$, where u, w are the horizontal and vertical velocity components) and vorticity ω (x, z, t) $(\omega = \psi_{xx} + \psi_{zz})$, takes the form

$$\omega_t + J(\omega, \psi) = g\rho_x/\rho + B(x, z, t) + D(x, z, t),$$

$$\rho_t + J(\rho, \psi) = (k_h\rho_x)_x + (k_v\rho_z)_z. \tag{1}$$

Here $\rho(x, z, t)$ is the water density, k_v and k_h are the coefficients of vertical and horizontal turbulent diffusion, $J(a, b) = a_x b_z - a_z b_x$ is the Jacobian operator and subscripted indices x, z, t denote partial derivatives with respect to the subscripted variable; $B(x, z, t)$ and $D(x, z, t)$ represent the non-Boussinesq and dissipative terms, respectively, and are given by

$$B(x, z, t) = \{-\rho_z[\psi_{xt} + J(\psi_z, \psi)] - \rho_x[\psi_{xt} + J(\psi_x, \psi)] + \rho_z[(a_h\psi_{xz})_x + (a_v\psi_{zz})_z] + \rho_x[(a_h\psi_{xx})_x + (a_v\psi_{xz})_z]\}/\rho,$$

$$D(x, z, t) = (a_h\psi_{xz})_{xz} + (a_h\psi_{xx})_{xx} + (a_z\psi_{zz})_{zz} + (a_h\psi_{xz})_{xz},$$

(Click the equation graphic to enlarge/reduce size)

where a_v and a_h are the coefficients of vertical and horizontal eddy viscosity. The non-Boussinesq terms were left in the governing system (1) to allow for a broader range of applicability although their influence on the dynamics of ISW turned out in our case not to be essential.

The coefficients, a_v and k_v are determined by the Richardson-number-dependent turbulent parameterizations like that of Pacanowski and Philander (1981), namely,

$$a_v = \frac{a_o}{[1 + \alpha Ri(x, z, t)]^p} + a_b,$$

$$k_v = \frac{a_o}{[1 + \alpha Ri(x, z, t)]^p} + k_b,$$

where the Richardson number is

$$Ri(x, z, t) = \frac{N^2(x, z, t)}{u_z^2(x, z, t)}.$$

Here a_b and k_b are dissipation parameters describing background turbulence and a_o, α, and p are adjustable parameters; N (x, z, t) is the local Brunt–Väisälä frequency ($N^2(x, z, t) = -g\rho_z/\rho$). These parameterizations for the vertical turbulent kinematic viscosity and diffusivity increase the coefficients a_v and k_v in regions with small values of Ri. In regions with vertical density inversions the Richardson number was taken to be 0.

The horizontal eddy viscosity a_h and turbulent diffusivity k_h are parameterized by

$$a_h = \beta_0 + \beta(\Delta x)^2|\partial u/\partial x|, \quad k_h = \mu_0 + \mu(\Delta x)^2|\partial u/\partial x|$$

(Stacey and Zedel 1986), where β_0 and μ_0 are homogeneous background values, β and μ are disposable parameters, and Δx is the horizontal step size of the grid.

We are interested in the baroclinic motions of the ocean, which is why we can use a rigid-lid condition at $z = 0$. In this case, at a free surface, the following boundary conditions can be selected:

$$\psi = 0, \quad \omega = 0, \quad \rho_z = 0. \tag{2}$$

The last two conditions denote the vanishing of the shear stresses and zero mass flux. The bottom line, $z = -H(x)$, is a streamline at which the no-slip condition and zero mass flux across the boundary are imposed:

$$\psi = 0, \quad \psi_z = \psi_x = 0, \quad \rho_n = 0, \tag{3}$$

where **n** is a normal vector to the irregular bottom relief. On the far-end vertical liquid boundaries, $x = \pm L$ (see Fig. 1a ⊙═), zero boundary conditions

$$\psi = 0, \qquad \omega = 0, \qquad \rho_x = 0 \qquad (4)$$

will be imposed; they require zero velocity and independence of the density field with x at $x = \pm L$ and will be assumed valid until wave disturbances reach these lateral boundaries.

System (1) with boundary conditions (2)–(4) was solved numerically. It was, however, useful first to perform a σ transformation of coordinates [$\sigma = -z/H(x)$], which transforms the physical domain with variable depth into a rectangular computational area. This allowed us to use a rectangular grid in the development of a numerical scheme.

The splitting-up method (Marchuk 1974) was applied for the finite difference approximation of the equations. The vorticity transport equation is integrated in time by splitting the temporal step into two semisteps. The spatial derivatives are approximated by means of second-order central finite differences. At each temporal semistep an implicit system of equations with a tridiagonal matrix is obtained that is solved using standard techniques. The streamfunction is then computed from the vorticity by solving the Poisson equation $\omega = \psi_{xx} + \psi_{zz}$, previously transformed with the use of the σ coordinate. For its solution a standard relaxation method is applied. Finally the density ρ is computed by using the same methodology as for the vorticity.

Several numerical experiments were performed to determine the values of the eddy viscosity and turbulent diffusivity parameters a_o, p, β_0, β, μ_0, μ. These calculations were done with the parameters listed in Table 1 ⊙═. It was found that by taking $\Delta t = 0.5$ s, $\Delta x = 2$ m, $\Delta z = 0.5$ m (in area III), $a_o = 10^{-3}$ m^2 s^{-1}, $p = 1$, $\beta_0 = 10^{-3}$ m^2 s^{-1}, $\beta = 10$, $\mu_0 = 10^{-4}$ m^2 s^{-1}, $\mu = 10$ the numerical scheme was quite stable even during the overturning of a wave front. At the same time the selection of these parameters provided a long distance propagation of ISW without essential attenuation (500 wavelength and more). This is in agreement with in situ observations, which show that ISW can propagate several hundred kilometers from the source of generation (Osborne and Burch 1980; Apel et al. 1985).

3. Model initialization

The background density distribution in the numerical runs was set by choosing the profiles typical for the Andaman and Sulu Seas (Levitus and Boyer 1994; Levitus et al. 1994), where large-amplitude solitary internal waves and their shoaling [and breaking, as in the Sulu Sea, (Chapman et al. 1991)] were observed (Fig. 1b ⊙═). The water depth H_1 in the deep part I of the basin was taken to be 1 km; in the shelf zone III, H_3 was constant and, in different runs, taken to have values between 200 and 100 m.

The approach we used here to obtain the initial fields for the incident wave in this paper was the same as that used in Vlasenko et al. (2000). At the first stage we considered a basin with constant depth H_1. The numerical model was initialized by using the first-mode analytical solitary wave solution of the stratified Korteweg-de Vries (KdV) equation. Such initial fields represent a stationary solitary wave solution in a weakly nonlinear, nonhydrostatic medium, but they do not satisfy the system (1) for large amplitude solitary waves, for which the nonlinear parameter lies outside the region of applicability of weakly nonlinear models. Once inserted in the numerical scheme the strong nonlinear wave will evolve in the basin of constant depth. During this evolutional process the initial large amplitude KdV soliton will be modified, and a new stationary solitary wave will be formed at the frontal side of the wave field. The leading wave with larger phase speed than the wave tail separates from the latter at a definite stage of evolution (at the distance of 20–30 wavelengths from its incept), and it independently propagates farther as a solitary wave. Thus, the model is run until a leading wave separates from the wave tail, and until a new stationary solution is reached at the frontal side of the wave field. This wave is then used as initial condition for the problem of the interaction of the intense ISW with the bottom topography.

Note that unlike the KdV solitons the ISWs of large amplitude have several specific features in their structure that increase with the growth of the wave amplitude. For instance, they are wider and propagate more slowly than the KdV solitons do. Furthermore, their vertical structure does not coincide exactly with the eigenfunctions of the linear boundary value problem of the vertical mode structure based on the given density structure. And, finally, the wavelength of large waves strongly depends on the vertical coordinate. For more details on the peculiarities of large solitary internal waves we refer the reader to the papers of Miyata (1985, 1988); Lamb and Yan (1996); Michallet and Barthelemy (1998), and Vlasenko et al. (2000).

In the present study the amplitudes a_m (maximum displacement of the isopycnals) of the incident internal waves of permanent form, defined for the profiles 1–3 in Fig. 1b ⊙═, were 19.2, 37.9, 57.6, 81.4, and 84.4 m.

4. Model results

Numerical experiments were carried out so as to model the interaction of large amplitude solitary internal waves with a slope–shelf area for the conditions of the Andaman and Sulu Seas. We did not choose any definite bottom profiles because of the wide variety of bottom topography occurring in these regions. Instead, we defined the transition zone II as a linear

slope region with inclination angle γ and performed numerical runs in a wide range of inclinations to make the results more applicable to different sites of the coastline. The slope angle γ varied from 0.52° to 21.8°.

a. Kinematics of wave breaking

More than 50 numerical runs were performed with the model parameters a_m, γ, H_3, and the buoyancy frequency profiles 1–3 listed above. Before describing the wave breaking criterion, which was found on the basis of the whole ensemble of model calculations, let us investigate a kinematic mechanism of overturning and strong breaking of internal waves with the use of one numerical run as an example. Different in detail, all breaking events nevertheless had similar features and peculiarities, which will be described now.

Figure 2 ⊙ displays the wave profile at three different time slices: far from the breaking zone (Fig. 2a ⊙), immediately before overturning (Fig. 2b ⊙), and during the breaking event (Fig. 2c ⊙). It should be mentioned here that a solitary wave with an amplitude of 84.4 m, propagating from the deep part of the basin ($H_1 = 1000$ m) over the slope with a relatively moderate inclination ($\gamma = 2.9°$), penetrates into the shallow zone (to the isobath of 260 m) without any essential change in its symmetry (Fig. 2a ⊙). Note that dispersive effects have not developed and a dispersive wave tail has not arisen at the downstream side of the wave. The solitary wave serves essentially as the wave profile until the isobath 250 m is reached. Only a weak wave asymmetry is discernible in the upper panel of Fig. 2 ⊙.

Starting at approximately $H = 250$ m the frontal face of the wave becomes more gently sloping and, correspondingly, the rear face becomes more steep. This behavior of wave shoaling, obtained here from direct numerical simulations, was also previously described in several experimental papers (e.g., Kao et al. 1985; Helfrich 1992; Michallet and Ivey 1999). Such a change of the wave profile occurs because of a smaller propagation velocity of a trough in comparison to the wave crest. This peculiarity of a shoaling of strong ISW deserves some comments.

Generally, according to the dependence of the local phase velocity on the fluid stratification, a deeper pycnocline leads to a larger internal wave speed (in a typical oceanic situation when the interface is closer to the free surface than to the bottom). For instance, in a two-layered system (with water density and thickness ρ_1, H_1 and ρ_2, H_2 for upper and lower layers, respectively) the linear phase speed is

$$C_p^{\text{lin}} = \left\{ g(\rho_2 - \rho_1)H_1 H_2 / [\rho_2(H_1 + H_2)] \right\}^{1/2}$$

in shallow water, or $C_p^{\text{lin}} = [g(\rho_2 - \rho_1)H_1/\rho_2]^{1/2}$ in deep water. Accordingly, the wave trough must propagate faster than the wave crest. Only when the pycnocline is located close to the bottom the situation changes to the opposite. Approximately such a scenario of internal wave evolution of different forms and origins (waves of depressions, long baroclinic tidal waves, etc.) was observed in the ocean and described in a series of theoretical papers by, for instance, Gerkema and Zimmerman (1995), Lamb (1994), Lamb and Yan (1996), Vlasenko (1992).

The aforementioned remark does not concern internal solitons. In the latest stages of evolution the wave field disintegrates into a series of ISW. In such waves nonlinearity and dispersion compensate each other; these waves propagate as waves of permanent form. Their trough and shoulders move with equal velocity despite their different distances to the free surface. This result is a consequence of weakly nonlinear theories (Benjamin 1966, 1967; Joseph 1977; Kubota et al. 1978; Benny 1966). The idea of the existence of ISW of permanent form beyond the limit of weakly nonlinear theories was also used in the present paper (section 3).

As was found in our study, a large amplitude ISW, propagating over a slowly variable depth, does not reveal any essential dispersive effects in the deep part of the ocean, as was expected. Over variable depth such waves adjust to the ambient conditions during the evolution without disintegration on a secondary wave tail (see also Grimshaw et al. 1999). Only starting at approximately 250 m depth the above described steepening of a rear wave face sets in. From this site (at $H < 250$ m) the ISW depresses the pycnocline below the middle of the water depth during propagation: isopycnal $\sigma_t = 3$ kg m^{-3}, which lies in the undisturbed fluid at a horizon of about 50 m falls down to additional 84.4 m in the wave center and reaches a horizon of about 134 m (see Figs. 2a,b ⊙).

The bottom panel in Fig. 2 ⊙ displays the isopycnal lines at the moment of overturning of a steep rear wave front; it shows that moment of time (Fig. 2c ⊙) when the top of the propagating baroclinic bore outstripped the wave trough. In this situation the heavier and denser water penetrates into the relatively light water layers and falls down to the wave trough. Thus, we may conclude that the reason for wave breaking is the kinematic instability of the wave profile.

Later we will dwell in more detail upon the analysis of this fact from the point of view of comparison of velocity of fluid particles (orbital velocities) and propagation speed (phase speed). Before, let us analyze the qualitative changes in the patterns of the horizontal and vertical velocities that take place during an overturning event. Figure 3 ⊙ represents the fields of density and u and w velocities at three different stages of the wave evolution: before overturning (Figs. 3a–c ⊙), just at the beginning of overturning (Figs. 3d–f ⊙), and after overturning (Figs. 3g–i ⊙). The striking feature of these patterns is the following: before breaking, the maximum of the horizontal velocity shifts from the free surface (where it was located in the initial wave) into the deep layers (to the wave trough, see Fig. 3b ⊙), and then shifts to the lateral boundary of the steep slope (see Fig. 3e ⊙), where the value of maximum velocity increases up to the wave breaking.

The overturning event is clearly seen also from the analysis of the evolution of the w field. Comparison of the three lower panels shows the appearance of downward water fluxes after the wave overturning (at position B in Fig. 3c 🔵➡) in a zone where otherwise upward fluxes of water exist.

The kinematic nature of the internal wave breaking described above becomes better understandable when horizontal velocity profiles are compared with the local phase speed of the wave. Figure 4 🔵➡ shows snapshots of $u(z)$ profiles corresponding to the vertical cross sections a–a, b–b, c–c, and d–d depicted in Figs. 3 and 4 🔵➡. Vertical dashed thin lines in Fig. 4 🔵➡ represent the local phase speed (which, in fact, diminishes with the shoaling of the wave). Before breaking a local maximum of both profiles a–a and b–b exists at depth (at $\bar{z} = 0.44$ and 0.57, respectively). Nevertheless, the magnitude of the velocity at this site is still less than the local wave speed. The next two profiles c–c and d–d reveal wave breaking. The magnitude of the horizontal velocity in the peaks exceeds the local phase speed.

So, as follows from the numerical runs, a *kinematic instability is responsible for the mechanism of strong wave breaking rather than a shearing instability,* as was suggested by Kao et al. (1985). Breaking of an internal wave arises on the steep rear slope of the wave at the location where onshore fluid velocities exceed the wave phase speed. Despite this fact, the possibility of attenuation and breaking of internal waves under the action of a shear instability should still not be neglected, as was found by Bogucki and Garret (1993) and also as our numerical experiments have shown. Figure 5 🔵➡ represents the fields of Richardson number Ri(x, z) computed for the initial incident wave in zone I (Fig. 5a 🔵➡) and just before wave breaking (Fig. 5b 🔵➡), corresponding to the situation displayed in Fig. 3d 🔵➡. The zone with Ri < 0.25 is rather small in the incident wave, just in the center of the solitary wave, and the minimum value of the Richardson number here does not drop below 0.2.

The situation is quite different at the instant of wave breaking. In the region of breaking (where the vertical fluid stratification is still stable) the Richardson number falls to the level 0.1, and the zone with Ri < 0.25 occupies a rather extended area. Thus, generation of shear instability and increasing turbulent mixing is very likely here, although, as was discussed and concluded above, the basic input for wave breaking is provided by the kinematic instability. Nevertheless, for a complete analysis existence of shear instability should also be taken into account.

Figure 6 🔵➡ represents the ultimate fate of a solitary wave after its breaking. As seen from the evolution of the density field the water does not mix instantaneously at the location of the overturned rear face. Observe, however, the formation of the "mushroom structures" at the beginning of the baroclinic bore breaking (Figs. 6b,c 🔵➡). The dense water, penetrating into the light layers, behaves as an upstream propagating jet. It undergoes multiple reflections from the near surface and near-bottom layer (Figs. 6c–e 🔵➡). At the latest stages of evolution the propagating jet gradually loses its coherent structure and transforms into a horizontal turbulent pulsating density current. In Fig. 7 🔵➡ this jet is presented in greater detail. It is characterized by the upslope directed core that is located in the intermediate layers and is exposed by vertical oscillations.

The above-considered peculiarities of the internal wave dynamics in the slope–shelf area can serve as explanation of some experimental evidences of the oceanic ISW breaking over inclined bottom topography. For instance, the shoreward flux (internal swash) was fixed near the shelf edge off the coast of Palawan Island in the Sulu Sea; this was the reason for a sudden shift of the CTD probe to the coast by the arrival of the upslope flow produced by the shoaling of the large solitary wave (Chapman et al. 1991). Besides, the inverse structure of the density presented in Fig. 7a 🔵➡ in the area of the upslope flux below the core was measured on the Pechora Sea Shelf after internal wave breaking had occurred (Serebryany and Shapiro 2000).

Note that the present example of overturning and strong breaking is one of the possible scenarios of the evolution of large amplitude ISW over the inclined bottom (probably the crucial one). Of course, intense ISW can penetrate onto the shelf also without destruction. The conditions of internal wave breaking are discussed below. In the latter case, when an ISW evolves in a shelf–slope area without overturning and when its parameters satisfy the conditions of weak nonlinearity, the evolution process can be investigated in the framework of the KdV equation. Essential progress in such an approach was recently achieved with the inclusion in the KdV equation of a quadratic as well as a cubic nonlinear term (see, e.g., Holloway et al. 1997, 1999). Due to the fact that the nonlinear and dispersion parameters of the KdV equation are very sensitive not only to the variations of bottom topography but also to the vertical stratification and to shear, the temporal and spatial changes of the latter (temporal and spatial variability of stratification and background currents) can lead to essential variations of the coefficients of the KdV equation (quadratic nonlinearity can even change its sign). The last circumstance leads to several interesting effects in the wave evolution (the resulting wave field significantly depends on the sign of the cubic nonlinear term and on the amplitude of the incoming wave). For more details see Grimshaw et al. (1999).

In this paper we focus attention only on the investigation of the mechanism of strong ISW breaking and conditions of its occurrence. Some other interesting effects were also found, which, however, are beyond the scope of the present study. For instance, the incoming wave in the transition area splits into transmitted and reflected waves, and this fission is more visible when $\gamma > 10°$. The characteristics of the wave field in the shallow water zone and the back radiated waves (their structure, amplitudes, modal composition) strongly depends on the bottom angle, parameter $H_3 - H_m$, position of the pycnocline, and wave amplitude. At large bottom inclination it is possible to generate not only first but also second mode secondary baroclinic waves (as transmitted, as reflected), solitons, and soliton trains. More details on this point can be found in the paper by Vlasenko and Hutter (2001).

b. Breaking criterion

From the numerical runs a breaking criterion was determined. It was found that, besides the slope angle, another basic parameter controlling the process whether a solitary wave passes into the shallow shelf zone III or will break somewhere over the slope region is the ratio of the wave amplitude a_m to $H_3 - H_m$, which is the distance from the undisturbed isopycnal of maximum amplitude (located at the depth H_m) to the bottom (see Fig. 1a ⌾ and insert in Fig. 8 ⌾).

Very often a two-layered approximation of water stratification is used for the analysis of oceanic solitary waves. In such a case the position of maximum amplitude coincides with the interface, and the value $H_3 - H_m$ is, in fact, the depth of the lower layer on the shelf. In our case (for a typical oceanic fluid stratification) the situation is more complicated and the maximum of the isopycnal depression lies below the seasonal pycnocline.

To estimate the expediency to use a two-layered approximation for the breaking criterion, note that the maximum of the vertical displacement eigenfunction for the above presented $N(z)$ profiles 1 and 2 with peaks at 48 and 78 m depth (see Fig. 1b ⌾) are located at horizons of 79 and 180 m, respectively. So, the depth of the maximum displacement in the two-layer model (if we define the position of buoyancy frequency maximum as an interface) and the continuously stratified model differ approximately by a factor of 2. As a consequence, all estimations obtained with the use of the parameter H_m in the two models will differ by about 100%. The situation is even worse for profile 3 in Fig. 1 ⌾. In this case, the pycnocline is very wide and has two local maxima. It is not evident where we should place the interface in a two-layered model if one tries to simplify the fluid stratification depicted by line 3. Probably a three-layered model is more appropriate in this case.

Thus, we define the value H_m as an undisturbed position of the isopycnal line that has maximum depression a_m at the center of the wave; see insert in Fig. 8 ⌾. Note, that H_m coincides with the depth H^{lin}_m of the eigenfunction maximum defined by the linear boundary value problem only in the limit of infinitesimal waves. For strongly nonlinear solitary internal waves the maximum of the wave amplitude (as found by Vlasenko et al. 2000) is shifted from the horizon $z = -H^{lin}_m$ and this shift increases with the growth of the wave amplitude.

The breaking criterion is shown in Fig. 8 ⌾ where $a_m/(H_b - H_m)$ is plotted against the slope angle γ. Only results with breaking events are presented here. The parameter H_b is the water depth at the point of wave breaking (see insert in Fig. 8 ⌾). The location of wave breaking, or the break point, was defined as the position where the orbital velocities begin to surpass the phase speed. Such an event is presented, for instance, in Figs. 3d–f ⌾.

One should note the close coincidence of the three curves obtained for the different density profiles. The best fit for these curves is curve 4 with the analytical representation

$$\bar{a} = \frac{a_m}{H_b - H_m} = \frac{0.8°}{\gamma} + 0.4, \qquad (5)$$

where γ is given in degrees. This curve separates the field of parameters $\bar{a}$, γ where breaking takes place (above the curve) from the region where the wave passes onto the shelf without breaking (below curve 4) if the point $[\gamma, a_m/(H_3 - H_m)]$ lies below curve 4.

The formulated breaking criterion for continuously stratified fluids generalizes the results obtained by Helfrich and Melville (1986) and Helfrich (1992) for a two-layered system. Over the range of parameters examined in those papers for laboratory conditions, breaking occurs where the undisturbed lower-layer depth was about 2–3 times a_m. They found that for $a_m/(H_b - H_m) < 0.3$ the incident wave moves onto the shelf without instabilities, and for $a_m/(H_b - H_m) > 0.4$ a strong overturning occurred above the slope. Their results were slightly dependent on the bottom angle.

In this connection one should mention a weak dependence of the wave breaking on the bottom angle also for a continuously stratified fluid in the range $\gamma > 5°$ (when the wavelength of the incident wave is comparable with the length of a transition zone). At the same time wave breaking strongly depends on the bottom angle when $\gamma < 5°$ (over the gently sloping bottom). This result was not cited previously and we will dwell on it in more detail.

The reason for such strong dependence consists in the dispersive effects that work together with nonlinearity. In the incident wave they compensate each other, and the initial wave propagates in the basin of constant depth as a solitary wave of permanent form. Over the inclined bottom this balance is violated and the solitary wave begins to change its shape. Over a short transition zone II ($\gamma > 5°$) the nonlinear effects predominate, and the incident wave is destroyed before the secondary waves can be radiated. For instance, one can indicate only a weak secondary wave in Figs. 2, 3, and 6 ⌾ behind the rear face of the overturning solitary wave (position A) as a manifestation of dispersion.

The situation is quite different when a solitary wave propagates over a gently sloping bottom. The example that illustrates this fact is presented in Fig. 9 ⌾. Because of a long propagation over a slightly inclined bottom a secondary wave tail has the possibility to evolve effectively because of dispersion. Position B in Fig. 9b ⌾ shows the initial stage of the wave tail development, and, finally, a well-developed wave train is clearly visible in Fig. 9d ⌾ (position C). A significant part of the

energy of the incident wave transfers to the dispersive wave tail. It can explain why larger waves can penetrate longer distances without breaking over the less inclined bottom. This effect is the more pronounced the more gently sloping the bottom topography is.

5. Summary and conclusions

In this paper some aspects of the evolution and transformation of internal solitary waves propagating in stratified water over the continental slope are discussed. A number of in situ and remote sensing measurements reveal that the shoaling effect and the local change of the bottom topography may essentially influence the dynamics of propagating waves. Attention in the present study was focused on the investigation of overturning and strong breaking of large amplitude waves over an inclined bottom. Such intense waves (with amplitudes up to 100 m and more) were observed in many sites of the World Ocean: in the Andaman Sea (Perry and Schimke 1965; Osborne and Burch 1980), in the Sulu Seas (Apel et al. 1985; Liu et al. 1985), at the Mascarene Ridge (Sabinin 1992; Konyaev et al. 1995), near the Straits of Giblartar (Bockel 1962; Bryden et al. 1994) and Messina (Vlasenko et al. 2000), and in the central Bay of Biscay (New and Pingree 1990), and the results of their breaking was measured in the Sulu Sea (Chapman et al. 1991) and the Pechora Seas (Serebryany and Shapiro 2000).

Unfortunately, this type of motion, especially the mechanism of wave breaking and conditions of its occurrence, has not been theoretically examined so far to a sufficient extent. A satisfactory theoretical description of wave breaking requires adequate simulation by use of numerical models based on a full nonlinear system of equations and cannot be considered in the frame of frequently exploited weakly nonlinear theories.

In the present study a numerical model, based on the Reynolds equations, was developed. It can reproduce the strongly nonlinear internal waves and their interaction with the bottom topography. The model is nonlinear, nonhydrostatic, and accounts for the real vertical fluid stratification, variable coefficients of vertical and horizontal turbulent exchange, and variable bottom topography. The basic goal of the numerical runs was to study the dynamics of internal solitary waves during its strong breaking, to describe the kinematics of wave overturning and to find the parameters that control wave breaking (the breaking criterion).

Numerical experiments were performed for the vertical fluid stratification and bottom parameters close to those observed in the Andaman and Sulu Seas where large amplitude waves and their shoaling were measured. The amplitudes of the incoming waves were 19.2, 37.9, 57.6, 81.4, and 84.4 m, the angle of the continental slope varied from 0.52° to 21.8°.

It was found that, when an intense ISW propagates from the deep part of a basin onto the shelf, a breaking event can arise if the waves amplitude a_m is larger than $0.4(H_s - H_m)$. In the shallow water zone the frontal face of the propagating wave becomes more gently sloping but the rear face becomes steeper. Such a change of the wave profile takes place because of the slower propagation velocity of a trough in comparison to the wave crest in the shallow water zone where the ISW depresses the pycnocline below the midwater depth. The cumulative effect of the nonlinearity leads to a steepening and overturning of the rear wave face over the inclined bottom. Just before breaking the horizontal orbital velocity at the site of instability exceeds the phase speed of the ISW. The top of the propagating baroclinic bore outstrips the wave trough and at this point the heavier and denser water penetrates into the relatively light water layers and cascades to the wave trough. So, the strong breaking is caused by a kinematic instability of the rear steep wave slope.

In the following stages of evolution of the overturned hydraulic jump, the water does not instantaneously mix at the place of the overturned rear wave face. The dense water behaves as an upstream propagating pulsating jet, penetrating into the light layers. It undergoes multiple reflections from the near-surface and near-bottom layer, and, at the latest stages of evolution, it gradually loses the coherent structure and transforms into a horizontal turbulent flux. It is characterized by the upslope directed core, which is located in the intermediate layers and is exposed by vertical oscillations.

The breaking criterion of ISWs over the sloping bottom (5) was found. Over the range of parameters examined in our study ($0.52° < \gamma < 21.8°$, where γ is the slope angle) the breaking event arises at the position with depth H_b when the nondimensional wave amplitude $\bar{a} = a_m / (H_b - H_m)$ satisfies the condition $\bar{a} \cong 0.8°/\gamma + 0.4$. If the water depth H_s on the shelf is less than H_b, a solitary wave breaks before it penetrates into the shallow water zone, otherwise (at $H_s > H_b$) it passes onto the shelf without breaking as a dispersive wave tail.

REFERENCES

Apel J. R., J. R. Holbrock, A. K. Liu, and J. J. Tsai, 1985: The Sulu Sea internal soliton experiment. *J. Phys. Oceanogr.*, **15**, 1625–1651.
Find this article online

Apel J. R., L. A. Ostrovsky, and Y. A. Stepanyants, 1995: Internal solitons in the ocean. Tech. Rep. MERCJRA0695, 70 pp. [Available from Milton S. Eisenhower Research Centre, Applied Physics Laboratory, The John Hopkins University, Johns Hopkins Rd., Laurel, MD 20707.].

Benjamin T. B., 1966: Internal waves of finite amplitude and permanent form. *J. Fluid Mech.*, **25**, 241–270. Find this article online

Benjamin T. B., 1967: Internal waves of permanent form in fluids of great depth. *J. Fluid Mech.*, **29**, 559–592. Find this article online

Benny D. J., 1966: Long nonlinear waves in fluids. *J. Math. Phys.*, **45**, 52–63. Find this article online

Bockel M., 1962: Travaux oceanographiques de l' "Origny" a Gibraltar. *Cah. Oceanogr.*, **14**, 325–329.

Bogucki D., and C. Garrett, 1993: A simple model for the shear-induced decay of an internal solitary wave. *J. Phys. Oceanogr.*, **23**, 1767–1776. Find this article online

Bryden H. L., J. Candela, and T. H. Kinder, 1994: Exchange through the strait of Gibraltar. *Progress in Oceanography,* Vol. 33, Pergamon Press, **33,** 201–248.

Cacchione D., and C. Wunsch, 1974: Experimental study of internal waves over a slope. *J. Fluid Mech.*, **66**, 223–239. Find this article online

Chapman D. C., G. S. Giese, M. G. Collins, R. Encarnacion, and G. Jacinto, 1991: Evidence of internal swash associated with Sulu Sea solitary waves? *Cont. Shelf Res.*, **11**, 591–599. Find this article online

De Silva I. P. D., J. Imberger, and G. N. Ivey, 1997: Localized mixing due to a breaking internal wave ray at a sloping bed. *J. Fluid Mech.*, **350**, 1–27. Find this article online

Diebels S., B. Schuster, and K. Hutter, 1994: Nonlinear internal waves over variable topography. *Geophys. Astrophys. Fluid Dyn.*, **76**, 165–192. Find this article online

Gerkema T., and J. T. F. Zimmerman, 1995: Generation of nonlinear internal tides and solitary waves. *J. Phys. Oceanogr.*, **25**, 1081–1094. Find this article online

Grimshaw R., E. Pelinovsky, and T. Talipova, 1999: Solitary wave transformation in a medium with sign-variable quadratic nonlinearity and cubic nonlinearity. *Physica D*, **132**, 4011–4062. Find this article online

Grue J., A. Jensen, P. O. Rusas, and K. J. Sveen, 2000: Breaking and broadening of internal solitary waves. *J. Fluid Mech.*, **413**, 181–217. Find this article online

Halpern D., 1971: Observations of short period internal waves in Massachusetts Bay. *J. Mar. Res.*, **29**, 116–132. Find this article online

Helfrich K. R., 1992: Internal solitary waves breaking and run-up on a uniform slope. *J. Fluid. Mech.*, **243**, 133–154. Find this article online

Helfrich K. R., and W. K. Melville, 1986: On long nonlinear waves over slope–shelf topography. *J. Fluid Mech.*, **167**, 285–308. Find this article online

Helfrich K. R., and J. W. Miles, 1984: On interfacial solitary waves over slowly varying topography. *J. Fluid Mech.*, **149**, 305–317. Find this article online

Holloway P. E., E. Pelinovsky, T. Talipova, and B. Barnes, 1997: A nonlinear model of internal tide transformation on the Australian North West shelf. *J. Phys. Oceanogr.*, **27**, 871–896. Find this article online

Holloway P. E., 1999: A generalized Korteweg–de Vries model of internal tide transformation in coastal zone. *J. Geophys. Res.*, **104**, 18333–18350. Find this article online

Ivey G. N., and R. I. Nokes, 1989: Vertical mixing due to the breaking of critical internal waves on sloping boundaries. *J. Fluid Mech.*, **204**, 479–500. Find this article online

Joseph R. I., 1977: Experimental study of solitary waves. *J. Phys. A: Math. Gen.*, **10**, 225–L227, L. Find this article online

Kao T. W., F. S. Pan, and D. Renouard, 1985: Internal solitons on the pycnocline: Generation, propagation, and shoaling and breaking over a slope. *J. Fluid. Mech.*, **159**, 19–53. Find this article online

Konyaev K. V., K. D. Sabinin, and A. Serebryany, 1995: Large amplitude internal waves at the Mascarene Ridge in the Indian Ocean. *Deep-Sea Res.*, **42**, 2075–2091. Find this article online

Kubota T., D. R. S. Ko, and A. Dobbs, 1978: Propagation of weakly nonlinear internal waves in a stratified fluid of final depth. *J. Hydronaut.*, **12**, 157–165. Find this article online

Lamb K. G., 1994: Numerical experiments on internal wave generation, by strongly tidal flow across a finite amplitude bank edge. *J. Geophys. Res.*, **99**, 843–864. Find this article online

Lamb K. G., and L. Yan, 1996: The evolution of internal wave undular bores: Comparison of fully nonlinear numerical model with weakly

nonlinear theory. *J. Phys. Oceanogr.*, **26**, 2712–2734. Find this article online

Lee C. Y., and R. Beardsley, 1974: The generation of long nonlinear internal waves in a weakly stratified shear flow. *J. Geophys. Res.*, **79**, 453–462. Find this article online

Levitus S., and T. P. Boyer, 1994: *Temperature*. Vol. 4, *World Ocean Atlas 1994,* NOAA Atlas NESDIS4, 117 pp.

Levitus S., R. Burgett, and T. P. Boyer, 1994: *Salinity*. Vol. 3, *World Ocean Atlas 1994,* NOAA Atlas NESDIS3, 99 pp.

Liu A. K., 1988: Analysis of nonlinear internal waves in the New York Bight. *J. Geophys. Res.*, **93**, 12317–12329. Find this article online

Liu A. K., L. R. Holbrook, and J. R. Apel, 1985: Nonlinear internal wave evolution in the Sulu Sea. *J. Phys. Oceanogr.*, **15**, 1613–1624. Find this article online

Liu A. K., Y. S. Chang, M.-K. Hsu, and N. K. Lang, 1998: Evolution of nonlinear internal waves in the East and South China Seas. *J. Geophys. Res.*, **103**, 7995–8008. Find this article online

Marchuk G. I., 1974: *Numerical Methods in Weather Prediction*. Academic Press, 277 pp.

Maurer J., K. Hutter, and S. Diebels, 1996: Viscous effects in internal waves of a two-layered fluid with variable depth. *Eur. J. Mech., B/Fluids*, **15**, 445–470. Find this article online

Maxworthy T., 1979: A note on the internal solitary waves produced by tidal flow over three-dimensional ridge. *J. Geophys. Res.*, **84**, 338–346. Find this article online

Michallet H., and E. Barthelemy, 1998: Experimental study of solitary waves, *J. Fluid Mech.*, **366**, 159–177. Find this article online

Michallet H., and G. M. Ivey, 1999: Experiments on mixing due to internal solitary waves breaking on uniform slopes. *J. Geophys. Res.*, **104**, 13467–13477. Find this article online

Miyata M., 1985: An internal solitary waves of large amplitude. *La Mer*, **23**, 43–48. Find this article online

Miyata M., 1988: Long internal waves of large amplitude. *Nonlinear Water Waves,* K. Horikawa, H. Maruo, Ed., Springer-Verlag, 399–406.

New A. L., and R. D. Pingree, 1990: Large amplitude soliton packets in the central Bay of Biscay. *Deep-Sea Res.*, **37A**, 513–524. Find this article online

Ono H., 1975: Algebraic solitary waves in stratified fluids. *J. Phys. Soc. Japan*, **39**, 1082–1091.

Osborne A. R., and T. I. Burch, 1980: Internal solitons in the Andaman Sea. *Nature*, **208**, 451–469. Find this article online

Ostrovsky L. A., and Y. A. Stepanyants, 1989: Do internal solitons exist in the ocean? *Rev. Geophys.*, **27**, 293–310. Find this article online

Pacanowski R. C., and S. G. H. Philander, 1981: Parameterization of vertical mixing in numerical models of tropical oceans. *J. Phys. Oceanogr.*, **11**, 1443–1451. Find this article online

Perry R. B., and G. R. Schimke, 1965: Large amplitude internal waves observed off the northwest coast of Sumatra. *J. Geophys. Res.*, **70**, 2319–2324. Find this article online

Sabinin K. D., 1992: Internal wave packets over the Maskaren ridge. *Izv. Akad. Sci. USSR, Atmos. Oceanic Phys.*, **28**, 625–633.

Saffarinia K., and T. W. Kao, 1996: A numerical study of the breaking of an internal soliton and its interaction with a slope. *Dyn. Atmos. Oceans*, **23**, 379–391. Find this article online

Serebryany A. N., and G. I. Shapiro, 2000: Overturning of soliton-like internal waves: Observations on the Pechora Sea Shelf. *Fifth Int. Symp. on Stratified Flows,* Vancouver, BC, Canada, University of British Columbia, 1029–1034.

Stacey M. W., and L. Zedel, 1986: The time-dependent hydraulic flow and dissipation over the sill of Observatory Inlet. *J. Phys. Oceanogr.*, **16**, 1062–1076. Find this article online

Stanton T. P., and L. A. Ostrovsky, 1998: Observations of highly nonlinear internal solitons over continental shelf. *Geophys. Res. Lett.*, **25**, 2695–2698. Find this article online

Terez D. E., and O. M. Knio, 1998: Numerical simulations of large-amplitude internal solitary waves. *J. Fluid Mech.*, **362**, 53–82. Find this article online

Thorpe S. A., 1999: The generation of alongslope currents by breaking internal waves. *J. Phys. Oceanogr.*, **29**, 29–38. Find this article online

Vlasenko V. I., 1992: Nonlinear model for the generation of baroclinic tides. *Phys. Oceanogr.*, **3**, 417–424. Find this article online

Vlasenko V. I., and K. Hutter, 2001: Generation of second mode solitary waves by the interaction of a first mode soliton with a sill. *Nonlinear Proc. Geophys.*, **8**, 1–17. Find this article online

Vlasenko V. I., P. Brandt, and A. Rubino, 2000: On the structure of large amplitude internal solitary waves. *J. Phys. Oceanogr.*, **30**, 2172–2185. Find this article online

Wallace B. C., and D. L. Wilkinson, 1988: Run-up of internal waves on a gentle slope in a two-layered system. *J. Fluid Mech.*, **191**, 419–442. Find this article online

Wessels F., and K. Hutter, 1996: Interaction of internal waves with a topographic sill in a two-layered fluid. *J. Phys. Oceanogr.*, **26**, 5–20. Find this article online

---

Tables

TABLE 1. List of the model parameters used in the numerical experiments

Parameter	Value
Δt (s)	0.2–2
Δx (m)	1–5
Δz (m) - shelf	0.25–1
a_o (m² s⁻¹)	(0.5–2) × 10⁻³
a_b (m² s⁻¹)	10⁻⁵
k_b (m² s⁻¹)	10⁻⁶
p	1; 2
β_o (m² s⁻¹)	10⁻³–10⁻⁵
β	0.1–50
μ_o (m² s⁻¹)	10⁻⁴–10⁻⁶
μ	0.1–50

Click on thumbnail for full-sized image.

Figures
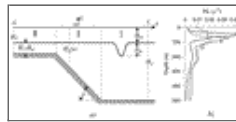
Click on thumbnail for full-sized image.

FIG. 1. Schematic diagram of the computational area (a); Buoyancy frequency profiles used in the model (b) measured in the Andaman Sea (1,2) and in the Sulu Sea (3)
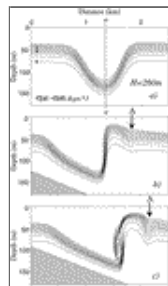
Click on thumbnail for full-sized image.

FIG. 2. The field of conventional density σ_t far from the breaking point (a); just before breaking (b), and after the overturning (c) of a rear wave face. The density contour interval is 0.5 kg m^{-3}. Position A indicates the secondary wave, generated behind the incoming wave. Section $a–a$ is used in connection with Fig. 4
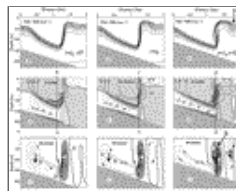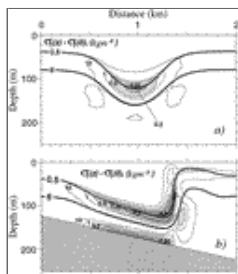

Click on thumbnail for full-sized image.

FIG. 3. Evolution of the conventional density σ_t (upper panels), horizontal velocity u (middle panels) and vertical velocity w (lower panels) during the breaking of internal solitary wave. The left column (a–c) represents the wave field before breaking, the middle column (d–f) just at the beginning of the overturning of a rear wave face, and the right column (g–i) after overturning. The timescale T equals 75.5 s. Black and white arrows show the downward and upward water fluxes, position A represents the secondary generated wave, position B shows the downward water flux at the site of wave breaking. Sections $b–b, c–c,$ and $d–d$ are used in connection with Fig. 4

FIG. 4. Vertical profiles of the horizontal velocity u normalized by the local phase speed c_p. Profiles were built for the cross sections a–a, b–b, c–c, and d–d, depicted in Figs. 2 and 3 ◉. (a) Corresponds to the vertical structure of the u velocity before wave breaking; (b) during overturning of the rear wave face
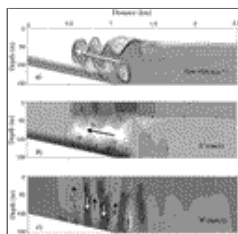
FIG. 5. Fields of the Richardson number calculated for the incident wave in the deep part of basin III (a) and over the slope area II just before wave breaking (b). The thick solid lines represent isopycnals 0.5 and 6.0
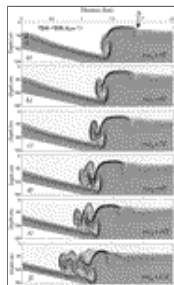
FIG. 6. The evolution of the density field during wave breaking. The contour interval equals 0.5 kg m^{-3}; the timescale T equals 75.5 s

FIG. 7. Fields of the conventional density σ_t (a), horizontal u (b) and vertical w (c) velocities 1057 s after breaking of the rear wave face. The contour interval for density equals 0.5 kg m^{-3}; those for horizontal and vertical velocities are presented in the figures. White and black arrows in (a) and (b) show the direction of propagation of the density intrusion. White and black arrows in (c) indicate downwelling and upwelling, respectively
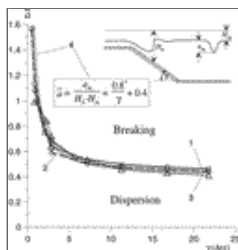
FIG. 8. Breaking events obtained in the model. Numbers of curves 1–3 correspond to the density profiles depicted in Fig. 1b ◉. The thick shaded line 4 is the best fit for the lines 1–3. It separates the fields of parameters for which internal wave breaking takes place (above the curve), or the wave passes onto the shelf as a dispersive wave train (below the curve). The sketch above explains the parameter used for the breaking criterion
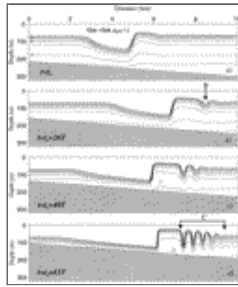
Click on thumbnail for full-sized image.

FIG. 9. Evolution of the density field over the genly sloping bottom ($\gamma = 0.52°$). The contour interval equals 0.5 kg m^{-3}, the timescale T equals 155 s. The secondary dispersive wave tail is shown by segment C in (d)

Corresponding author address: Vasiliy Vlasenko, Institut für Mechanik, Technische Universität Darmstadt, Hochschulstr. 1, D-64289 Darmstad, Germany. E-mail: vasiliy@mechanik.tu-darmstadt.de

top ▲